HHS Public Access

Author manuscript

J Mol Cell Cardiol. Author manuscript; available in PMC 2023 June 01.

Published in final edited form as:

J Mol Cell Cardiol. 2022 June ; 167: 1–14. doi:10.1016/j.yjmcc.2022.03.002.

EFHD1 ablation inhibits cardiac mitoflash activation and protects cardiomyocytes from ischemia

David R. Eberhardt[1], **Sandra H. Lee**[1], **Xue Yin**[1], **Anthony M. Balynas**[1], **Emma C. Rekate**[1], **Jackie N. Kraiss**[1], **Marisa J. Lang**[2], **Maureen A. Walsh**[2], **Molly E. Streiff**[1,3], **Andrea C. Corbin**[1,3], **Ying Li**[5], **Katsuhiko Funai**[2], **Frank B. Sachse**[1,3], **Dipayan Chaudhuri**[1,4]

[1]Nora Eccles Harrison Cardiovascular Research and Training Institute (CVRTI), University of Utah

[2]Diabetes & Metabolism Research Center, University of Utah

[3]Department of Biomedical Engineering, University of Utah

[4]Department of Internal Medicine, Division of Cardiovascular Medicine, University of Utah, Salt Lake City, Utah

[5]Nutrition and Integrative Physiology, University of Utah, Salt Lake City, Utah

Abstract

Altered levels of intracellular calcium (Ca^{2+}) are a highly prevalent feature in different forms of cardiac injury, producing changes in contractility, arrhythmias, and mitochondrial dysfunction. In cardiac ischemia-reperfusion injury, mitochondrial Ca^{2+} overload leads to pathological production of reactive oxygen species (ROS), activates the permeability transition, and cardiomyocyte death. Here we investigated the cardiac phenotype caused by deletion of *EF-hand domain-containing protein D1* (*Efhd1*$^{-/-}$), a Ca^{2+}-binding mitochondrial protein whose function is poorly understood. *Efhd1*$^{-/-}$ mice are viable and have no adverse cardiac phenotypes. They feature reductions in basal ROS levels and mitoflash events, both important precursors for mitochondrial injury, though cardiac mitochondria have normal susceptibility to Ca^{2+} overload. Notably, we also find that *Efhd1*$^{-/-}$ mice and their cardiomyocytes are resistant to hypoxic injury.

INTRODUCTION

Mitochondrial dysfunction commonly occurs during the progression of heart failure [1]. In healthy hearts, calcium (Ca^{2+}) regulates mitochondrial metabolism, morphology, and trafficking [2, 3]. In heart disease, however, excess Ca^{2+} entry into mitochondria causes increased pathological reactive oxygen species (ROS) production, leading to the mitochondrial permeability transition (MPT)[4, 5]. During the MPT, a large channel opens,

CORRESPONDING AUTHOR: Dipayan Chaudhuri, MD, PhD, dipayan.chaudhuri@hsc.utah.edu, 95 South 2000 East, Cardiovascular Research and Training Institute, University of Utah, Salt Lake City, UT, (801) 585-3682.

DISCLOSURES

None

collapsing the mitochondrial inner membrane potential ($\Delta\Psi$), disrupting mitochondrial function, and causing cardiomyocyte death and heart failure.

We sought to investigate novel targets involved in cardiac mitochondrial Ca^{2+} and ROS signaling. In a recent study, the EF-hand domain-containing protein D1 (EFHD1) was identified as a Ca^{2+}-sensor for mitoflash activation [6]. Mitoflashes are transient and discreet mitochondrial depolarizations associated with a respiratory and ROS burst [7, 8]. Increased mitoflash activity is known to presage MPT. Thus, proteins that regulate mitoflash production may constitute novel targets or pathways for therapies to prevent cardiac injury.

There has been limited study of EFHD1. It is a 27 kDa protein consisting of two Ca^{2+}-binding EF-hand domains and a protein-binding coiled-coiled domain [9]. In its initial characterization, it was found to localize predominantly to mitochondria, possibly the inner mitochondrial membrane [10], while structurally-similar homologs EFHD2 and allograft inflammatory factor-1 (AIF), localize to the cytoplasm [11]. In humans, variation in EFHD1 predicts circulating liver enzyme levels [12]. EFHD1 is also a marker of differentiated state lost in certain cancers [13–15], and its expression increases when an important component of the mitochondrial anti-oxidant system, superoxide dismutase 2, is downregulated [16]. In studies of *Efhd1*$^{-/-}$ mice, lowered basal respiration and ATP production were noted in the dorsal root ganglion [17]. A slight increase in peripheral neuronal cell death was noted, though functional consequences appeared absent. Mitochondrial function was also altered in pro-B immune cells after EFHD1 inhibition, with a shift towards glycolysis [18]. These studies provide a partial picture, which suggests that EFHD1 is involved in mitochondrial metabolism at the interface between ROS and Ca^{2+}.

In the present study, we describe the cardiac phenotype of *Efhd1*$^{-/-}$ mice. We found that *Efhd1*$^{-/-}$ mice displayed no overt cardiac pathology, while ROS and mitoflash activity was decreased. We also found that *Efhd1*$^{-/-}$ mice are resistant to hypoxia and cell death due to ischemia at baseline. The paucity of baseline phenotypes present in *Efhd1*$^{-/-}$ animals suggests it may be safe to target this molecule or its regulatory pathway for cardioprotection.

METHODS

Animal handling and genotyping

All animal procedures have been reviewed and approved by the Institutional Animal Care and Use Committee at the University of Utah. *Efhd1*$^{-/-}$ mice were obtained from the Jackson Laboratory (Bar Harbor, ME, C57BL/6NJ-Efhd1$^{em1(IMPC)J}$/Mmjax). Animals were kept on a C57BL/6NJ background. Animals were housed under standard conditions and allowed free access to food and water. Mice were euthanized via CO_2 inhalation, with an intermediate check at 4 mins. All mice used for analysis were young adults (7–18 weeks). For echocardiography and histology mice were all 18 weeks of age.

Echocardiography

Echocardiography was performed on 18-week old mice. Mice were initially sedated with 2% inhaled isoflurane (Vet One, NDC13985–046-60) anesthetic. They were restrained in the supine position and fur was cleared from the chest with a depilatory gel, after which

anesthesia was lowered. Warmed ultrasound gel was applied to the animal and 2D, M-mode and Doppler images were recorded in short-axis at the level of the papillary muscles, using a Vevo 2100 ultrasound machine equipped with a 55-MHz probe (Visual Sonics, Toronto, Ontario, Canada).

Mitochondrial isolation

Mice were euthanized as described above and the organs were removed and washed in ice-cold phosphate buffered saline (PBS). Hearts were rapidly dissected to remove atria and great vessels, and then placed in ice-cold initial medium containing (mM): 225 mannitol, 70 sucrose, 5 HEPES, 1 EGTA, and 0.1% (w/v) bovine serum albumin (BSA), and 1 μM thapsigargin (TG) (pH to 7.2 with KOH; osmolality to 290–310 mOsm/L). Tissue was homogenized using a Potter-Elvehjem tissue grinder attached to an overhead stirrer (IKA, Wilmington, NC) for 10–15 strokes at 180 rpm. The homogenate was centrifuged at 700 × *g* for 7 minutes and the tissue pellet was discarded. The supernatant was then centrifuged at 8500 × *g* for 10 minutes to obtain a mitochondrial fraction. The mitochondrial pellet was washed twice with and carefully resuspended, using a pipette tip where the end had been removed, in imaging solution containing (mM): 125 KCL, 20 HEPES, 5 K_2HPO_4, 1 $MgCl_2$, and 10 μM EGTA (pH to 7.2 with KOH, osmolality 290–300 mOsm/L). Protein concentration was quantified using the Pierce 660 nm Protein Assay Reagent (Thermo Fisher, Waltham, MA) according to the manufacturer's directions. In each subsequent assay, we obtained parallel data from knockout and littermate or age- and sex-matched C57BL/6NJ WT controls processed together. This isolation protocol was not geared towards isolating any particular subfraction of cardiomyocyte mitochondrial populations, e.g. subsarcolemmal versus intermyofibrillar.

Isolation of other organelles

For differential centrifugation experiments to study non-mitochondrial organelles, we followed a secondary protocol described previously [19]. Mouse organs were harvested and homogenized as described above for mitochondrial isolation. The homogenate was first spun at 600 × *g* for 3 minutes at 4°C. The pellet contained nuclei and cell debris. The supernatant was taken and spun at 6,000 × *g* for 10 minutes. The pellet contained the mitochondrial and lysosomal fraction. The supernatant was taken and spun at 40,000 × *g* for 30 minutes using a Beckman Coulter® Optima™ MAX-XP bench-top Ultracentrifuge. The pellet contained microsomes from the ER. The supernatant was taken and spun at 100,000 × *g* for 90 minutes. The pellet contained light microsomes from the endoplasmic reticulum (ER) and ribosomes. The supernatant contained the cytosolic fraction. Purity of each fraction was confirmed via Western Blot using antibodies against known organelle marker proteins.

Isolation of mitochondrial-associated membranes (MAMs)

MAMs were isolated as described previously [20]. Briefly, the crude mitochondrial pellet was obtained. The crude mitochondria were then layered on top of Percoll medium, consisting of (mM): 225 mannitol, 25 HEPES, 1 EGTA, 30% Percoll (pH 7.4). The crude mitochondria and Percoll medium were spun at 95,000 × *g* for 30 minutes at 4°C. After the spin, a dense band containing pure mitochondria was located at the bottom of the tube, and a dense band containing MAM was visible above the mitochondrial band. The bands were

extracted and spun at 6,300 × *g* for 10 minutes at 4°C. The mitochondrial fraction was then collected. The MAM fraction was spun again at 100,000 × g for 1 hour and the pure MAM collected. Purity of each fraction was confirmed via Western Blot using antibodies against known organelle marker proteins.

Proteinase K assay

Mitochondrial fractions were subject to a proteinase K assay as described previously[21, 22]. Mitochondria were resuspended in a sucrose buffer (200 mM sucrose, 10 mM Tris-MOPS, 1 mM EGTA-Tris) to a final concentration of 1 mg/ml. 20 μg of mitochondria were treated with digitonin (0.0001–1%, Sigma) or RIPA (150 mM NaCl, 50 mM Tris-HCL, 1% (w/v) Triton X-100, 0.5 % (w/v) deoxycholic acid, 0.1 % (w/v) sodium dodecyl sulfate (SDS), pH 7.8) and 100 μg/ml of proteinase K (New England Biolabs, Ipswich, MA) for 15 min at room temperature, in a 30 μl final volume. Proteinase K was then inhibited by addition of 5 mM phenylmethylsulfonyl fluoride (PMSF). 5 μg of protein was loaded to Tris-glycine gels for Western blotting.

Western blots

Tissue was lysed in RIPA supplemented with protease and phosphatase inhibitors (Thermo Fisher) and then mixed in a 1:1 ratio with Western blot loading dye (4X Bolt™ LDS Sample Buffer supplemented with 10 mM Dithiothreitol (DTT). Protein concentration was quantified by BCA assay (Thermo Fisher). 5–20 μg of protein from total heart lysates were loaded on polyacrylamide gels and processed as described previously on PVDF membranes[23]. We used the following antibodies: β-actin (ab8224, Abcam, Cambridge, MA, 1:1000 dilution), Calreticulin (D3E6, Cell Signaling Technology [CST], Danvers, MA, 1:1000 dilution), GAPDH (14C10, CST, 1:1000 dilution), HA-Tag (C29F4, CST, 1:1000), MCU (D2Z3B, CST, 1:1000 dilution), NDUFS3 (ac14711, Abcam, 1:1000 dilution), PPIF (ac110324, Abcam, 1:1000 dilution), PRELID1 (ab196275, Abcam, 1:1000 dilution), TOMM20 (D8T4N, CST, 1:1000 dilution), pan-voltage-dependent anion channel (VDAC, D73D12, CST, 1:1000 dilution). Band intensity was analyzed using ImageJ[24]. Expanded views of all membranes are available in Fig. S1–S3.

The EFHD1 rabbit polyclonal antibody a rabbit was developed by Pacific Immunology, (Ramona, CA). Rabbits were immunized with the EFHD1 peptide sequence: Cys-EQEERKREEEARRLRQAAFRELKAAFSA (Mouse *Efhd1* 212–240). The EFHD1 polyclonal antibody was used at a concentration of 1:500 for Western blot analysis. The antibody was validated by testing against Efhd1−/− mouse tissue (Figure 2B–D).

Co-Immunoprecipitation

HAP1 cells were grown and transfected with either an EFHD1-HA construct, or an OMP25-GFP-HA construct (a gift from David Sabatini, Addgene plasmid # 83356) [25]. Cells were then harvested and lysed in a PBS solution containing 1 % Triton-x-100 and 10 mM phenylmethylsulfonyl fluoride (PMSF) by passing through a 25G needle. The lysates were quantified using a BCA assay and diluted to 250 μg/mL of protein. 500 μL of the lysates were agitated in 20 μL of EZview™ Rd Anti-HA Affinity Gel beads (Sigma, E6779)

overnight at 4°C. The beads were washed four times in PBS+1% Triton-X-100 before being mixed 1:1 with western blot loading dye and loaded on a gel for western blot analysis.

ΔΨ imaging

For measurement of ΔΨ, 100 μg of mitochondria were incubated in 100 μL imaging solution supplemented with (mM): 5 L-glutamic acid, 5 L-malic acid and 50 nM tetramethylrhodamine methyl ester (TMRM, Thermo Fisher) for 10 minutes. We collected baseline signal for 1 minute, then injected 5 μM carbonyl cyanide 4-trifluoromethoxyphenylhydrazone (FCCP), and calculated the maximal change in TMRM signal at excitation and emission wavelengths of 548/574 nm [26]. Imaging was performed in 96-well plates on a Cytation 5 microplate reader.

Cardiomyocyte isolation and imaging

Mice were euthanized with CO_2 and their hearts subsequently extracted via thoracotomy. The ascending aorta was cannulated on a 25-gauge blunt needle. Cardiomyocytes were obtained by retrograde perfusion with Collagenase II (1.2 g/L, Worthington Biochemical Corporation, Lakewood, NJ) and Protease XIV (0.1 g/L, Sigma), and stored in a 0.5 mM Ca^{2+} HEPES-buffered saline solution. Isolated cardiomyocytes were resuspended in warm modified KHB buffer containing (mM): 138.2 NaCl, 0.0037 KCl, 0.0012 KH_2PO_4, 1.2 $MgSO_4$.7 H_2O, 15 Glucose, 21.85 HEPES (1% BSA, pH 7.2). Cells were then subjected to increasing Ca^{2+} concentrations (0.063 mM, 0.125 mM,0.25 mM, 0.5 mM, and 1 mM) and loaded with 20 nM TMRM, 5 μM MitoSox (Thermo Fisher), or 5 μM X-Rhod1 (Thermo Fisher) for 30 minutes at 37°C and then placed in glass-bottomed chamber (MatTek, MA) and mounted on the stage of a Zeiss LSM 510 confocal microscope (Peabody, MA). All three dyes were measured with an excitation and emission at 548/574 nm. All cells were imaged at the same power and gain settings. Image analysis was performed using Cell Profiler [27].

Mitoflash imaging

Cardiomyocytes were isolated as above and subsequently placed into KHB buffer containing (mM): 138.2 NaCl, 0.0037 KCl, 0.0012 KH_2PO_4, 1.2 $MgSO_4$.7 H_2O, 15 Glucose, 21.85 HEPES (1% BSA, pH 7.2) supplemented with either 0.25 CaCl2, or 1 mM $CaCl_2$ and 50 nM TMRM and incubated for 30 minutes at 37°C. Cardiomyocytes were then placed in a glass-bottomed chamber (MatTek, MA) on the stage of a Zeiss LSM 510 confocal microscope (Zeiss, Oberkochen, Germany). Cells were imaged at excitation and emission 548/574 nm for 100 s at a 512 by 32 pixel resolution and scanning frequency of 1000 Hz. Mitoflashes were identified as a transient loss of brightness in TMRM signal. Individual mitoflashes were counted by eye as described previously [28].

Cardiac histology and immunohistochemistry

Cardiac extraction from animals was as described above for cardiomyocyte isolation. The heart was subsequently incubated in a fixative solution containing 4% paraformaldehyde in PBS for 48 hours at 4°C and then placed in a 70% ethanol solution. The samples were embedded in paraffin, cut, and stained by the Research Histology core at the Huntsman

Cancer Institute (University of Utah) and ARUP Research Institute (Salt Lake City, Utah). Staining was for Masson's trichrome.

Calcium retention capacity (CRC)

Imaging was performed in 96-well plates on a Cytation 5 microplate reader. 100 μg of mitochondria were incubated in 100 μL of imaging solution supplemented with (mM): 5 L-glutamic acid, 5 L-malic acid, and 20 μM TMRM. Excitation and emission wavelengths were 548/574 nm. Bolus injections of 5 μM $CaCl_2$ were injected into each well every 5 minutes for 60 minutes. CRC was analyzed by calculating the amount of Ca^{2+} added to each well before an MPT event was observed.

Mitochondrial respiration (OXPHOS).

Pellets from the mitochondrial isolation step were suspended in buffer Z (MES potassium salt; 105 mM, KCl 30 mM, KH_2PO_4 10 mM, $MgCl_2$ 5 mM, and BSA 0.5 mg/ml), and analyzed by high-resolution respirometry (Oroboros O_2k Oxygraphs) to determine substrate-dependent respiration. Respiration was measured in response to the following substrate concentrations: 0.5 mM malate, 5 mM pyruvate, 2 mM ADP, 10 mM succinate, and 1.5 μM FCCP, as described previously [29]. Respiration rates were normalized to total protein content. Respiratory acceptor control ratio (RCR) was calculated as State 3/State 4 respiration [30]. For whole cardiomyocyte respirometry, mouse cardiomyocytes were isolated as described above and resuspended in KHB buffer supplemented with 1 mM Na-pyruvate (Thermo) to a final concentration of 2.5E5 cells/mL. Respiration was measured in response to the following substrate concentrations: 1.5 μM Oligomycin, 1.5 μM FCCP, 1 μM Rotenone/Antimycin A. Concentrations were titrated for optimum response.

Ischemia/reperfusion protocol for neonatal mouse cardiomyocytes.

A glucose-free, serum-free "ischemic" cell media was made using Dulbecco's modified eagle's medium (DMEM) without glucose, L-glutamine, phenol red, sodium pyruvate or sodium bicarbonate (Sigma, D5030). Potassium concentration of the media was doubled by adding 0.4 g/L KCl and pH was adjusted to 6.5 to simulate typical ischemic conditions of hyperkalemia and acidosis. The "ischemic" DMEM was gassed with 95% nitrogen, 5% carbon dioxide for 1 hr prior to use to expel any excess oxygen.

Neonatal mouse ventricular myocytes (NMVMs) were isolated from 1–2 day old mice following Pierce™ primary isolation kit (88281, Thermo Fisher Scientific). After 72 hours in standard culture conditions, the NMVM media was replaced with "ischemic" DMEM and plates were placed in a sealed contained at 37 °C with constant gas flow of 95% nitrogen, 5% carbon dioxide to ensure complete depletion of oxygen from culture. After 4 hours in "ischemia," NMVMs were washed and normal DMEM was replaced. NMVMs were left in cell culture incubator for 24 hours for a period of "reperfusion."

For Live/Dead analysis, cells were washed twice in PBS then incubated at room temperature in a PBS solution containing 100 μM 4′,6′-diamidino-2-phenylindole (DAPI) as described previously [31, 32]. Cells were then imaged using a Cytation 5 microplate reader on area-scan mode at excitation and emission of 358/461 nm. The fluorescence levels were

normalized to a blank well. A well where the cells had been killed using 10% (v/v) Dimethyl sulfoxide (DMSO) was used as a reference for 100% cell mortality. The fluorescent signal from ischemic cells was compared with non-ischemic controls which were treated in the same way minus exposure to ischemic conditions.

Ischemia/reperfusion protocol for adult cardiomyocytes.

Adult cardiomyocytes were isolated as described above and then placed in a sealed container at 37 °C with constant gas flow of 95% nitrogen, 5% carbon dioxide to ensure complete depletion of oxygen from the solution. Ischemia lasted for either 2 hours (ROS measurements), or 30 mins (mitoflash measurements). Following ischemia, cells were removed from the container and measurements were taken either immediately (<30 mins post ischemia) or at 2 hours post ischemia. Control cells were kept at 37°C for the same amount of time that the experimental cells were exposed to ischemic conditions.

Statistical analysis

Microsoft Excel and OriginPro (OriginLab) were used for data analysis. We rejected the null hypothesis for P values < 0.05. For comparison tests on samples where $n < 15$, we established used a Mann-Whitney statistical test. For comparisons on samples > 15, we used a two-tailed, unequal variance, Student's t-test. For the analysis of contingency tables, we performed a Fisher's exact test using Prism (GraphPad Software).

RESULTS

EFHD1 localizes to the mitochondrial outer membrane and intermembrane space

We obtained a custom-made rabbit polyclonal antibody targeting an internal sequence common to human and mouse EFHD1. In agreement with the initial report [10], we detected EFHD1 at high levels in brain and kidney mitochondria. It was also present at detectable levels in adult (>8 weeks old) heart and skeletal muscle, with somewhat lower levels in lung and liver mitochondria (Figure 1A). We confirmed EFHD1 is enriched in mitochondrial fractions following differential centrifugation. Notably, we also found EFHD1 in both the ER and cytosolic fractions (Figure 1B).

Furthermore, and contrary to previous findings, our data suggest that EFHD1 is not a mitochondrial inner membrane protein. To examine subcellular location, we performed a proteinase K assay. In this test, mitochondria isolated from mouse kidney were exposed to increasing concentrations of digitonin and assayed for enzymatic digestion with proteinase K. At low concentrations, digitonin will only permeabilize the outer mitochondrial membrane, exposing proteins at the outer membrane and within the intermembrane space to degradation. At higher concentrations, digitonin will also break down the inner mitochondrial membrane, exposing proteins at the inner membrane and within the matrix to degradation. We found that EFHD1 underwent an initial large degradation similar to the outer mitochondrial membrane protein TOMM20 and then a secondary breakdown mimicking PRELID1, a protein in the intermembrane space (Figure 1C). This suggests that EFHD1 resides on the outer membrane and within the intermembrane space of mitochondria. To further confirm this, we used differential ultracentrifugation to

isolate mitochondrial membranes which associate with the ER (mitochondria-associated membranes), which constitute purely outer membrane fractions. We found that EFHD1 was present in these ER-associated mitochondrial membranes in a similar way to voltage-dependent anion channels (VDAC), an outer mitochondrial membrane protein (Figure 1D). Finally, if EFHD1 is on the outer membrane, we reasoned that EFHD1 may interact with outer membrane proteins. VDACs are outer membrane proteins which allow Ca^{2+} to pass across the outer mitochondrial membrane. We therefore performed co-immunoprecipitation by transfecting HAP1 cells with a HA-tagged EFHD1 protein, using another outer membrane protein (OMP25-HA) as control. We found that VDAC co-immunoprecipitated with EFHD1-HA but not OMP25, suggesting that EFHD1 can bind outer mitochondrial membrane proteins (Figure 1E). These data all suggest that EFHD1 is a mitochondrial protein primarily associated with the mitochondrial outer membrane and intermembrane space.

Efhd1$^{-/-}$ mice are viable

Having established the localization of EFHD1, we characterized basic cardiac phenotypes of the whole-body *Efhd1*$^{-/-}$ mouse, obtained from the Jackson Laboratory (Figure 2A). Our antibody effectively distinguished wild-type versus *Efhd1*$^{-/-}$ in heart, liver and kidney tissue (Figure 2B–D). We found no difference in physical size between age- and sex-matched WT and *Efhd1*$^{-/-}$ mice (Figure 2E). Moreover, we also measured body weight and tibia length of WT and *Efhd1*$^{-/-}$ mice and found no difference in these features (Figures 2F–2I).

Efhd1$^{-/-}$ mice exhibit normal cardiac function

We next focused on cardiac function in the *Efhd1*$^{-/-}$ mice. We performed physical measurements, echocardiography and histology on hearts from 18-week old WT and *Efhd1*$^{-/-}$ mice. We found no difference in the appearance of hearts from WT and *Efhd1*$^{-/-}$ mice (Figure 3A), and tissue histology was also similar, with no evidence of increased fibrosis (Figure 3B–C). We found no difference in the absolute or normalized weights of the mouse hearts (Figure 3D, F, G). Additionally, we found no age-related differences in the heart weight/tibia length ratio of mice (Figure 3H). The International Mouse Phenotyping Consortium analyzed electrocardiographic parameters in these mice, and found no difference compared to WT animals [33].

Next, we tested for differences in basic cardiac function. We performed echocardiograms on 18-week old male and female WT and *Efhd1*$^{-/-}$ mice from three separate litters. Representative traces from a WT and *Efhd1*$^{-/-}$ mouse are shown in Figure 3I–L. We found no significant differences in fractional shortening (Figure 3M), E/A ratio (Figure 3N) or in E/E’ ratio (Figure 3O), markers of systolic and diastolic function. We also found no differences between left ventral diameter and wall thickness in both systole (Figure 3P–R) and diastole (Figure 3S–U). We therefore concluded that the absence of EFHD1 in mice did not result in any overt cardiomyopathy.

We next focused on characterizing the effect of EFHD1 absence on mitochondrial function. We did not see any difference in mitochondrial protein yield between WT and *Efhd1*$^{-/-}$ hearts (Figure 3E). Decreased respiration levels have previously been reported

in dorsal root ganglion cells from *Efhd1*$^{-/-}$ mice [17]. We therefore used an Oroboros O_2K-FluoRespirometer to measure respiration rates in mitochondria isolated from WT and *Efhd1*$^{-/-}$ mouse hearts. Figure 4A and 4B shows representative traces obtained from WT and *Efhd1*$^{-/-}$ heart mitochondria, respectively. We did not find differences in Complex I-linked respiration; OXPHOS capacity of complex I, driven by NADH related substrates; maximal OXPHOS capacity with convergent input through both complex I and complex II; maximal convergent respiratory capacity; or respiratory efficiency, measured as the respiratory control ratio (Figure 4C) [34, 35]. Similarly, when measuring respiration in whole cardiomyocytes in the presence of inhibitors, we found no differences in basal respiration, ATP-linked respiration, proton leak or in maximal respiration (Figure 4D–I). Taken together, this suggests that EFHD1 ablation does not alter basal cardiac mitochondrial function.

Efhd1$^{-/-}$ mice have diminished mitochondrial Ca^{2+}, ROS, and mitoflash levels

Next, we examined mitochondrial Ca^{2+} levels, and found that baseline concentrations were significantly lower in isolated Efhd1$^{-/-}$ cardiomyocytes, when compared with WT cells (Figure 5A and 5B).

Prior experiments in HeLa cells[6] suggested EFHD1 knockdown decreased the frequency of mitoflashes, transient depolarizations stimulated by increased mitochondrial ROS, which are potential precursors of MPT. Thus, we were interested in testing the effect of deleting EFHD1 on Ca^{2+}-overload induced MPT, since EFHD1 is a Ca^{2+} sensor. We used the Ca^{2+}retention capacity (CRC) assay, in which purified mitochondria are repeatedly challenged with Ca^{2+} boluses until MPT activation causes depolarization and Ca^{2+} release. We found no difference in cardiac CRC (Figures 5C, D) or expression of mitochondrial Ca^{2+} uptake proteins (Figure 5E, F), between WT and *Efhd1*$^{-/-}$ mitochondria.

Since ROS can trigger MPT and mitochondrial dysfunction independent of Ca^{2+} overload, we next examined these by measuring mitoflashes and ROS levels. Mitoflashes were manually counted over 100s as described previously [28]. In concordance with the prior study, we found that *Efhd1−/−* cardiomyocytes exhibited significantly fewer mitoflashes than WT (Figure 6A). Moreover, ROS-sensitive MitoSox dye levels were significantly decreased in *Efhd1*$^{-/-}$ cardiac mitochondria (Figure 6B, 6C) consistent with the reduction in mitoflashes. Indeed, diminished ROS levels in *Efhd1*$^{-/-}$ cardiomyocytes was maintained at higher extracellular Ca^{2+} levels (Figures 6A and 6B), or when cardiomyocytes were stressed via β-adrenergic stimulation with isoproterenol (Figure 6E).

Mitoflash and ROS production is intimately related to membrane potential ($\Delta\Psi$), with increased hyperpolarization tending to produce more ROS [7, 8, 36]. Thus, we examined $\Delta\Psi$ in *Efhd1*$^{-/-}$ cardiomyocytes using potentiometric TMRM dye. We found that TMRM staining was diminished, suggesting a more depolarized $\Delta\Psi$, relative to WT cells. This effect is consistent with the lowered ROS and mitoflash production seen above.

Efhd1$^{-/-}$ mice are resistant to hypoxia

In performing our assays, we noticed that *Efhd1*$^{-/-}$ mice took much longer to euthanize with CO_2 when compared with their WT counterparts. Our protocol involves exposing mice

to CO_2 continuously in an enclosed chamber, checking their status at 4 minutes, which in littermate WT mice leads to 100% mortality. However, we were surprised to find that 50% of our *Efhd1*$^{-/-}$ mice were still alive at 4 mins (Figure 7A), often requiring 7 to 8 minutes. To examine if a similar effect could be reproduced in cardiac tissue, we isolated neonatal mouse ventricular myocytes (NMVMs) from *Efhd1*$^{-/-}$ heart. We collected NMVMs from 1-day old WT and *Efhd1*$^{-/-}$ pups and exposed half of the cells to a deoxygenated, high-potassium, low-pH media for 4 hours, mimicking ischemic conditions, while the other half remained in normal media. Subsequently, cells were grown for 24 hours in regular oxygenated media, to mimic reperfusion, after which the amount of dead cells in each condition was quantified. We found that NMVMs from *Efhd1*$^{-/-}$ were twice as resistant to cell death when exposed to ischemic conditions compared to their WT counterparts (Figure 7B). We then sought to confirm this in adult cardiomyocytes. We therefore exposed isolated adult cardiomyocytes from WT and *Efhd1*$^{-/-}$ mouse hearts to simulated ischemia followed by reperfusion and measured mitochondrial ROS levels and mitoflash frequencies. We measured ROS levels immediately following ischemia and following 2 hours of reperfusion. As expected, ROS levels increased in cells exposed to ischemia and reperfusion. Notably, this increase in ROS was significantly blunted in *Efhd1*$^{-/-}$ compared to WT cardiomyocytes whether measurements were taken immediately after ischemia (Figure 7C) or after 2 hours of reperfusion (Figure 7D). Similarly, the decreased mitoflashes observed at baseline in *Efhd1*$^{-/-}$ cardiomyocytes was maintained following ischemia-reperfusion (Figure 7E). Taken together, our results suggest *Efhd1*$^{-/-}$ mice are resistant to cardiomyocyte cell death, possibly through a mechanism involving mitochondrial ROS production.

DISCUSSION

Here, we present the initial characterization of the baseline cardiac phenotype of *Efhd1*$^{-/-}$ mice. The major conclusions are that *Efhd1*$^{-/-}$ mice (1) do no display any obvious organismal or cardiac pathology at baseline, (2) cardiomyocyte ROS and ROS-dependent mitoflashes are decreased, and (3) at the organismal and cardiomyocyte level, they are resistant to hypoxic cell death.

EFHD1 resides on the outer membrane and intermembrane space of mitochondria

In this study, we used a knockout-validated EFHD1 antibody to demonstrate that that EFHD1 resides primarily on the outer mitochondrial membrane, with lower protein levels being present in the intermembrane space (Figure 1C). This was confirmed using differential centrifugation, a proteinase K protection assay, and purification of ER-associated mitochondrial outer membranes. EFHD1 possesses no transmembrane domains, so it is likely only associated with membranes, rather than an integral component. At first glance, this finding appears contrary to previously findings, which report EFHD1 is an inner membrane protein [10]. However, there has been little investigation of EFHD1 function, and its subcellular localization has been directly examined in only the initial report [10]. In that report, inner membrane localization was assigned based on an immunostaining showing colocalization with a mitochondrial marker, and an immunogold assay showing enrichment in inner membrane on electron microscopy. However, there are two strong caveats related to that evidence. First, even in that report, the authors described substantial EFHD1 staining

outside the inner membrane in several other figures. In fluorescent immunostaining, EFHD1 was seen in cytoplasm, neurites, and growth cones. In immunogold staining, although there was greatest labeling of the inner membrane, there is also a diffuse pattern of staining throughout mitochondria and other locations. Second, the authors report that, on western blotting, their rabbit polyclonal antibody detects several non-specific bands. Thus, it is unclear if the staining seen with fluorescence or electron microscopy is entirely specific to EFHD1. Because we also found substantial non-specific bands using our antibody, we limited our analysis to western blots, where we have validated the specific band using *Efhd1*$^{-/-}$ mouse tissues.

Independent evidence also suggests that EFHD1 is primarily associated with the outer membrane protein. In a study using BioID proximity ligation to map mitochondrial proteomic interactions, EFHD1 was found as a bait primarily with BioID-tagged outer membrane proteins, such as *MAVS, MTCH2,* and *MFN2* [37]. Separately, a structural study revealed that EFHD1 alters cytoskeletal actin polymerization, which would accessible only from the outer membrane [9]. Finally, EFHD1 lacks a canonical mitochondrial targeting sequence, common among inner membrane and matrix proteins. Taken together, results here are best reconciled with prior evidence if EFHD1 primarily resides in the mitochondrial outer membrane and intermembrane space, with its reputed inner membrane localization possibly a consequence of looser associations from the intermembrane space with integral inner membrane proteins, rather than a restricted or constitutive inner membrane localization.

EFHD1 ablation does not produce an overt cardiac phenotype, but is associated with lowered cardiac mitochondrial ROS levels and resistance to hypoxic death

We found no adverse effects of EFHD1 ablation on organismal growth, cardiac function, and cardiac mitochondrial respiration. This stands in contrast to studies performed in sensory neurons and differentiating B cells, where a reduction in mitochondrial metabolism and shift towards glycolysis was noted [17, 18]. Part of the effect may be due to the levels of EFHD1, which are higher in neurons compared to cardiomyocytes, though even within the nervous system there were apparently minimal functional deficits.

The production of mitochondrial ROS is often a byproduct of respiratory flux and occurs mainly in the matrix and inner membrane. Yet, despite no change in cardiac mitochondrial respiration, we observed a robust reduction in mitochondrial ROS levels. Similarly, mitoflashes, the ROS-dependent respiratory bursts producing transient mitochondrial depolarization, were decreased by more than half in *Efhd1*$^{-/-}$ cardiomyocytes, with many cells producing none at all[8]. This result is consistent with prior data showing diminished mitoflash frequency in HeLa cells depleted of EFHD1 [6]. In addition, we find lower levels of mitochondrial Ca^{2+} and membrane potential, not seen in the prior study, possibly due to cell type or the use of siRNA rather than full knockout as performed here. Furthermore, the discrepancy between decreased ROS despite unaltered respiration suggests that EFHD1 may be influencing the mitochondrial anti-oxidant response. Indirect evidence for this comes from prior studies showing that alterations in the levels of Superoxide Dismutase 2, an important mitochondrial enzyme for detoxifying excess superoxide anions, are countered by

opposing changes in *EFHD1* expression [16]. The molecular mechanism by which EFHD1, residing outside the matrix, alters the function of mitochondrial ROS production, is likely indirect and remains to be determined, though the effect appears reproducible across several cell types.

Mitoflashes are thought to be precursors to the MPT, as excess ROS is a potent trigger for this event. We would therefore expect that mitochondria lacking *Efhd1* would be less susceptible to Ca^{2+}-induced MPT. However, when performing the standard Ca^{2+} retention capacity assays, we found unchanged sensitivity in *Efhd1*$^{-/-}$ hearts (Figure 6C, D). This finding was surprising and suggests that mitochondrial sensitivity to ROS can be altered independently of its susceptibility to Ca^{2+} overload. One caveat is that CRC assays were performed on isolated mitochondria. If EFHD1 is involved with interactions between the mitochondrial outer membrane and other organelles, such as the ER, the limitations of studying the mitochondria in isolation needs to be taken into account.

Our data shows that EFHD1 is localized at the intermembrane space and at the outer mitochondrial membrane, where it associates with VDAC proteins or other outer membrane proteins [37]. VDAC channels are critical for cardiac Ca^{2+} signaling and ROS generation [38–40]. We have also shown here that ablation of EFHD1 decreases ROS levels, mitochondrial Ca^{2+} levels, and mitoflashes in isolated cardiomyocytes, so we speculate that EFHD1 may affect ROS levels through its interaction with VDAC or other outer membrane proteins. Because the primary sites of mitochondrial ROS production are within the inner membrane at Complex I and III, EFHD1 effects are likely indirect, and EFHD1-mediated alterations in Ca^{2+} uptake could lead to enhanced ROS production by boosting NADH input into the electron transport chain, affecting antioxidant systems, or altering susceptibility to the MPT [36, 41–44].

Arguably the most profound phenotype which we report here is the resistance to CO_2 euthanasia exhibited by *Efhd1*$^{-/-}$ mice and the corresponding resistance to ischemia-reperfusion in isolated cardiomyocytes. This finding is intriguing, because it suggests the decreased ROS and mitoflash production in *Efhd1*$^{-/-}$ cardiomyocytes may lead to a resistance to ischemic injury at the organismal level.

Because our results have shown that EFHD1 ablation produces no obvious cardiac pathology, targeting this protein or its interactions may be a safe intervention providing a potentially novel therapy for cardiac injury.

Limitations

Our intent in this study was to provide an initial characterization of the baseline cardiac phenotype in *Efhd1*$^{-/-}$ mice. It is unclear if the effects on ROS and cell death will translate to cardioprotection during different forms of cardiac injury. As we could not measure cardiac function during the euthanasia protocol, we cannot definitively establish that the tolerance to CO_2 are due to changes in ROS production as seen in the ischemia-reperfusion assays. In addition, having determined that EFHD1 is primarily resident on the outer membrane and intermembrane space, the precise molecular mechanism by which it transduces the effects on ROS remains unexplained. Finally, it is also possible that changes

in other organ systems, such as previously noted changes in neurons, may also contribute to the phenotypes observed here [17].

Supplementary Material

Refer to Web version on PubMed Central for supplementary material.

Acknowledgments

We wish to thank Emma Eberhardt for her help in mitoflash analysis.

SOURCES OF FUNDING

This work was supported by the Heart, Lung, and Blood Institute of the NIH under award R01HL141353 (D.C.), American Heart Association under Postdoctoral Fellowship award 834544(D.E.), Larry H. Miller Driving Out Diabetes Initiative (D.C.), and the Nora Eccles Treadwell Foundation (D.C.). The content is solely the responsibility of the authors and does not necessarily represent the official views of the funding agencies.

REFERENCES

[1]. Zhou B, Tian R, Mitochondrial dysfunction in pathophysiology of heart failure, J Clin Invest 128(9) (2018) 3716–3726. [PubMed: 30124471]

[2]. Glancy B, Balaban RS, Role of mitochondrial Ca2+ in the regulation of cellular energetics, Biochemistry 51(14) (2012) 2959–73. [PubMed: 22443365]

[3]. Jeyaraju DV, Cisbani G, Pellegrini L, Calcium regulation of mitochondria motility and morphology, Biochim Biophys Acta 1787(11) (2009) 1363–73. [PubMed: 19138660]

[4]. Kwong JQ, Molkentin JD, Physiological and pathological roles of the mitochondrial permeability transition pore in the heart, Cell Metab 21(2) (2015) 206–214. [PubMed: 25651175]

[5]. Moris D, Spartalis M, Spartalis E, Karachaliou GS, Karaolanis GI, Tsourouflis G, Tsilimigras DI, Tzatzaki E, Theocharis S, The role of reactive oxygen species in the pathophysiology of cardiovascular diseases and the clinical significance of myocardial redox, Ann Transl Med 5(16) (2017) 326. [PubMed: 28861423]

[6]. Hou T, Jian C, Xu J, Huang AY, Xi J, Hu K, Wei L, Cheng H, Wang X, Identification of EFHD1 as a novel Ca(2+) sensor for mitoflash activation, Cell Calcium 59(5) (2016) 262–70. [PubMed: 26975899]

[7]. Wang W, Fang H, Groom L, Cheng A, Zhang W, Liu J, Wang X, Li K, Han P, Zheng M, Yin J, Wang W, Mattson MP, Kao JP, Lakatta EG, Sheu SS, Ouyang K, Chen J, Dirksen RT, Cheng H, Superoxide flashes in single mitochondria, Cell 134(2) (2008) 279–90. [PubMed: 18662543]

[8]. Wang X, Jian C, Zhang X, Huang Z, Xu J, Hou T, Shang W, Ding Y, Zhang W, Ouyang M, Wang Y, Yang Z, Zheng M, Cheng H, Superoxide flashes: elemental events of mitochondrial ROS signaling in the heart, J Mol Cell Cardiol 52(5) (2012) 940–8. [PubMed: 22405973]

[9]. Mun SA, Park J, Park KR, Lee Y, Kang JY, Park T, Jin M, Yang J, Jun CD, Eom SH, Structural and Biochemical Characterization of EFhd1/Swiprosin-2, an Actin-Binding Protein in Mitochondria, Front Cell Dev Biol 8 (2020) 628222. [PubMed: 33537316]

[10]. Tominaga M, Kurihara H, Honda S, Amakawa G, Sakai T, Tomooka Y, Molecular characterization of mitocalcin, a novel mitochondrial Ca2+-binding protein with EF-hand and coiled-coil domains, J Neurochem 96(1) (2006) 292–304. [PubMed: 16336229]

[11]. Dütting S, Brachs S, Mielenz D, Fraternal twins: Swiprosin-1/EFhd2 and Swiprosin-2/EFhd1, two homologous EF-hand containing calcium binding adaptor proteins with distinct functions, Cell Commun Signal 9 (2011) 2. [PubMed: 21244694]

[12]. Chambers JC, Zhang W, Sehmi J, Li X, Wass MN, Van der Harst P, Holm H, Sanna S, Kavousi M, Baumeister SE, Coin LJ, Deng G, Gieger C, Heard-Costa NL, Hottenga JJ, Kuhnel B, Kumar V, Lagou V, Liang L, Luan J, Vidal PM, Mateo Leach I, O'Reilly PF, Peden JF, Rahmioglu N, Soininen P, Speliotes EK, Yuan X, Thorleifsson G, Alizadeh BZ, Atwood LD, Borecki IB, Brown

MJ, Charoen P, Cucca F, Das D, de Geus EJ, Dixon AL, Doring A, Ehret G, Eyjolfsson GI, Farrall M, Forouhi NG, Friedrich N, Goessling W, Gudbjartsson DF, Harris TB, Hartikainen AL, Heath S, Hirschfield GM, Hofman A, Homuth G, Hypponen E, Janssen HL, Johnson T, Kangas AJ, Kema IP, Kuhn JP, Lai S, Lathrop M, Lerch MM, Li Y, Liang TJ, Lin JP, Loos RJ, Martin NG, Moffatt MF, Montgomery GW, Munroe PB, Musunuru K, Nakamura Y, O'Donnell CJ, Olafsson I, Penninx BW, Pouta A, Prins BP, Prokopenko I, Puls R, Ruokonen A, Savolainen MJ, Schlessinger D, Schouten JN, Seedorf U, Sen-Chowdhry S, Siminovitch KA, Smit JH, Spector TD, Tan W, Teslovich TM, Tukiainen T, Uitterlinden AG, Van der Klauw MM, Vasan RS, Wallace C, Wallaschofski H, Wichmann HE, Willemsen G, Wurtz P, Xu C, Yerges-Armstrong LM, C. Alcohol Genome-wide Association, R. Diabetes Genetics, S. Meta-analyses, C. Genetic Investigation of Anthropometric Traits, C. Global Lipids Genetics, C. Genetics of Liver Disease, P. International Consortium for Blood, G. Meta-analyses of, C. Insulin-Related Traits, Abecasis GR, Ahmadi KR, Boomsma DI, Caulfield M, Cookson WO, van Duijn CM, Froguel P, Matsuda K, McCarthy MI, Meisinger C, Mooser V, Pietilainen KH, Schumann G, Snieder H, Sternberg MJ, Stolk RP, Thomas HC, Thorsteinsdottir U, Uda M, Waeber G, Wareham NJ, Waterworth DM, Watkins H, Whitfield JB, Witteman JC, Wolffenbuttel BH, Fox CS, Ala-Korpela M, Stefansson K, Vollenweider P, Volzke H, Schadt EE, Scott J, Jarvelin MR, Elliott P, Kooner JS, Genome-wide association study identifies loci influencing concentrations of liver enzymes in plasma, Nat Genet 43(11) (2011) 1131–8. [PubMed: 22001757]

[13]. Lucas B, Grigo K, Erdmann S, Lausen J, Klein-Hitpass L, Ryffel GU, HNF4alpha reduces proliferation of kidney cells and affects genes deregulated in renal cell carcinoma, Oncogene 24(42) (2005) 6418–31. [PubMed: 16007190]

[14]. Mandruzzato S, Callegaro A, Turcatel G, Francescato S, Montesco MC, Chiarion-Sileni V, Mocellin S, Rossi CR, Bicciato S, Wang E, Marincola FM, Zanovello P, A gene expression signature associated with survival in metastatic melanoma, J Transl Med 4 (2006) 50. [PubMed: 17129373]

[15]. Shukla R, Upton KR, Munoz-Lopez M, Gerhardt DJ, Fisher ME, Nguyen T, Brennan PM, Baillie JK, Collino A, Ghisletti S, Sinha S, Iannelli F, Radaelli E, Dos Santos A, Rapoud D, Guettier C, Samuel D, Natoli G, Carninci P, Ciccarelli FD, Garcia-Perez JL, Faivre J, Faulkner GJ, Endogenous retrotransposition activates oncogenic pathways in hepatocellular carcinoma, Cell 153(1) (2013) 101–11. [PubMed: 23540693]

[16]. Hurt EM, Thomas SB, Peng B, Farrar WL, Molecular consequences of SOD2 expression in epigenetically silenced pancreatic carcinoma cell lines, Br J Cancer 97(8) (2007) 1116–23. [PubMed: 17895890]

[17]. Ulisse V, Dey S, Rothbard DE, Zeevi E, Gokhman I, Dadosh T, Minis A, Yaron A, Regulation of axonal morphogenesis by the mitochondrial protein Efhd1, Life Sci Alliance 3(7) (2020).

[18]. Stein M, Dütting S, Mougiakakos D, Bösl M, Fritsch K, Reimer D, Urbanczyk S, Steinmetz T, Schuh W, Bozec A, Winkler TH, Jäck HM, Mielenz D, A defined metabolic state in pre B cells governs B-cell development and is counterbalanced by Swiprosin-2/EFhd1, Cell Death Differ 24(7) (2017) 1239–1252. [PubMed: 28524857]

[19]. Rosenberg IM, Protein analysis and purification: Benchtop Techniques (Second Edition), Second ed., Birkhauser, Boston1996.

[20]. Wieckowski MR, Giorgi C, Lebiedzinska M, Duszynski J, Pinton P, Isolation of mitochondria-associated membranes and mitochondria from animal tissues and cells, Nat Protoc 4(11) (2009) 1582–90. [PubMed: 19816421]

[21]. Baughman JM, Perocchi F, Girgis HS, Plovanich M, Belcher-Timme CA, Sancak Y, Bao XR, Strittmatter L, Goldberger O, Bogorad RL, Koteliansky V, Mootha VK, Integrative genomics identifies MCU as an essential component of the mitochondrial calcium uniporter, Nature 476(7360) (2011) 341–5. [PubMed: 21685886]

[22]. Chaudhuri D, Sancak Y, Mootha VK, Clapham DE, MCU encodes the pore conducting mitochondrial calcium currents, Elife 2 (2013) e00704. [PubMed: 23755363]

[23]. Sommakia S, Houlihan PR, Deane SS, Simcox JA, Torres NS, Jeong MY, Winge DR, Villanueva CJ, Chaudhuri D, Mitochondrial cardiomyopathies feature increased uptake and diminished efflux of mitochondrial calcium, J Mol Cell Cardiol 113 (2017) 22–32. [PubMed: 28962857]

[24]. Schneider CA, Rasband WS, Eliceiri KW, NIH Image to ImageJ: 25 years of image analysis, Nat Methods 9(7) (2012) 671–5. [PubMed: 22930834]

[25]. Chen WW, Freinkman E, Wang T, Birsoy K, Sabatini DM, Absolute Quantification of Matrix Metabolites Reveals the Dynamics of Mitochondrial Metabolism, Cell 166(5) (2016) 1324–1337.e11. [PubMed: 27565352]

[26]. Sancak Y, Markhard AL, Kitami T, Kovács-Bogdán E, Kamer KJ, Udeshi ND, Carr SA, Chaudhuri D, Clapham DE, Li AA, Calvo SE, Goldberger O, Mootha VK, EMRE is an essential component of the mitochondrial calcium uniporter complex, Science 342(6164) (2013) 1379–82. [PubMed: 24231807]

[27]. McQuin C, Goodman A, Chernyshev V, Kamentsky L, Cimini BA, Karhohs KW, Doan M, Ding L, Rafelski SM, Thirstrup D, Wiegraebe W, Singh S, Becker T, Caicedo JC, Carpenter AE, CellProfiler 3.0: Next-generation image processing for biology, PLoS Biol 16(7) (2018) e2005970. [PubMed: 29969450]

[28]. Li A, Qin Y, Gao M, Jiang W, Liu B, Tian X, Gong G, Protocol for Imaging of Mitoflashes in Live Cardiomyocytes, STAR Protoc 1(2) (2020) 100101. [PubMed: 33111128]

[29]. Johnson JM, Ferrara PJ, Verkerke ARP, Coleman CB, Wentzler EJ, Neufer PD, Kew KA, de Castro Brás LE, Funai K, Targeted overexpression of catalase to mitochondria does not prevent cardioskeletal myopathy in Barth syndrome, J Mol Cell Cardiol 121 (2018) 94–102. [PubMed: 30008435]

[30]. Chance B, Williams GR, Respiratory enzymes in oxidative phosphorylation. I. Kinetics of oxygen utilization, J Biol Chem 217(1) (1955) 383–93. [PubMed: 13271402]

[31]. Cummings BS, Schnellmann RG, Measurement of cell death in mammalian cells, Curr Protoc Pharmacol Chapter 12 (2004) Unit 12.8.

[32]. Chaudhuri D, Artiga DJ, Abiria SA, Clapham DE, Mitochondrial calcium uniporter regulator 1 (MCUR1) regulates the calcium threshold for the mitochondrial permeability transition, Proc Natl Acad Sci U S A 113(13) (2016) E1872–80. [PubMed: 26976564]

[33]. Dickinson ME, Flenniken AM, Ji X, Teboul L, Wong MD, White JK, Meehan TF, Weninger WJ, Westerberg H, Adissu H, Baker CN, Bower L, Brown JM, Caddle LB, Chiani F, Clary D, Cleak J, Daly MJ, Denegre JM, Doe B, Dolan ME, Edie SM, Fuchs H, Gailus-Durner V, Galli A, Gambadoro A, Gallegos J, Guo S, Horner NR, Hsu CW, Johnson SJ, Kalaga S, Keith LC, Lanoue L, Lawson TN, Lek M, Mark M, Marschall S, Mason J, McElwee ML, Newbigging S, Nutter LM, Peterson KA, Ramirez-Solis R, Rowland DJ, Ryder E, Samocha KE, Seavitt JR, Selloum M, Szoke-Kovacs Z, Tamura M, Trainor AG, Tudose I, Wakana S, Warren J, Wendling O, West DB, Wong L, Yoshiki A, MacArthur DG, Tocchini-Valentini GP, Gao X, Flicek P, Bradley A, Skarnes WC, Justice MJ, Parkinson HE, Moore M, Wells S, Braun RE, Svenson KL, de Angelis MH, Herault Y, Mohun T, Mallon AM, Henkelman RM, Brown SD, Adams DJ, Lloyd KC, McKerlie C, Beaudet AL, Bućan M, Murray SA, High-throughput discovery of novel developmental phenotypes, Nature 537(7621) (2016) 508–514. [PubMed: 27626380]

[34]. Long Q, Huang L, Huang K, Yang Q, Assessing Mitochondrial Bioenergetics in Isolated Mitochondria from Mouse Heart Tissues Using Oroboros 2k-Oxygraph, Methods Mol Biol 1966 (2019) 237–246. [PubMed: 31041752]

[35]. Sjövall F, Ehinger JK, Marelsson SE, Morota S, Frostner EA, Uchino H, Lundgren J, Arnbjörnsson E, Hansson MJ, Fellman V, Elmér E, Mitochondrial respiration in human viable platelets--methodology and influence of gender, age and storage, Mitochondrion 13(1) (2013) 7–14. [PubMed: 23164798]

[36]. Wei L, Dirksen RT, Perspectives on: SGP symposium on mitochondrial physiology and medicine: mitochondrial superoxide flashes: from discovery to new controversies, J Gen Physiol 139(6) (2012) 425–34. [PubMed: 22641637]

[37]. Antonicka H, Lin ZY, Janer A, Aaltonen MJ, Weraarpachai W, Gingras AC, Shoubridge EA, A High-Density Human Mitochondrial Proximity Interaction Network, Cell Metab 32(3) (2020) 479–497.e9. [PubMed: 32877691]

[38]. DeHart DN, Fang D, Heslop K, Li L, Lemasters JJ, Maldonado EN, Opening of voltage dependent anion channels promotes reactive oxygen species generation, mitochondrial dysfunction and cell death in cancer cells, Biochem Pharmacol 148 (2018) 155–162. [PubMed: 29289511]

[39]. Liu N, Li Y, Nan W, Zhou W, Huang J, Li R, Zhou L, Hu R, Interaction of TPPP3 with VDAC1 Promotes Endothelial Injury through Activation of Reactive Oxygen Species, Oxid Med Cell Longev 2020 (2020) 5950195. [PubMed: 33082910]

[40]. Shankar TS, Ramadurai DKA, Steinhorst K, Sommakia S, Badolia R, Thodou Krokidi A, Calder D, Navankasattusas S, Sander P, Kwon OS, Aravamudhan A, Ling J, Dendorfer A, Xie C, Kwon O, Cheng EHY, Whitehead KJ, Gudermann T, Richardson RS, Sachse FB, Schredelseker J, Spitzer KW, Chaudhuri D, Drakos SG, Cardiac-specific deletion of voltage dependent anion channel 2 leads to dilated cardiomyopathy by altering calcium homeostasis, Nat Commun 12(1) (2021) 4583. [PubMed: 34321484]

[41]. Brookes PS, Yoon Y, Robotham JL, Anders MW, Sheu SS, Calcium ATP, and ROS: a mitochondrial love-hate triangle, Am J Physiol Cell Physiol 287(4) (2004) C817–33. [PubMed: 15355853]

[42]. Batandier C, Leverve X, Fontaine E, Opening of the mitochondrial permeability transition pore induces reactive oxygen species production at the level of the respiratory chain complex I, J Biol Chem 279(17) (2004) 17197–204. [PubMed: 14963044]

[43]. Chen Q, Vazquez EJ, Moghaddas S, Hoppel CL, Lesnefsky EJ, Production of reactive oxygen species by mitochondria: central role of complex III, J Biol Chem 278(38) (2003) 36027–31. [PubMed: 12840017]

[44]. Feng G, Liu B, Li J, Cheng T, Huang Z, Wang X, Cheng HP, Mitoflash biogenesis and its role in the autoregulation of mitochondrial proton electrochemical potential, J Gen Physiol 151(6) (2019) 727–737. [PubMed: 30877142]

HIGHLIGHTS

- EFHD1 localizes to the mitochondrial outer membrane and intermembrane space
- *Efhd1*$^{-/-}$ mice exhibit normal cardiac function
- *Efhd1*$^{-/-}$ mice have reduced mitochondrial Ca^{2+}, $\Delta\Psi$, ROS, and mitoflash levels
- *Efhd1*$^{-/-}$ mouse cardiomyocytes are resistant to ischemia-reperfusion injury

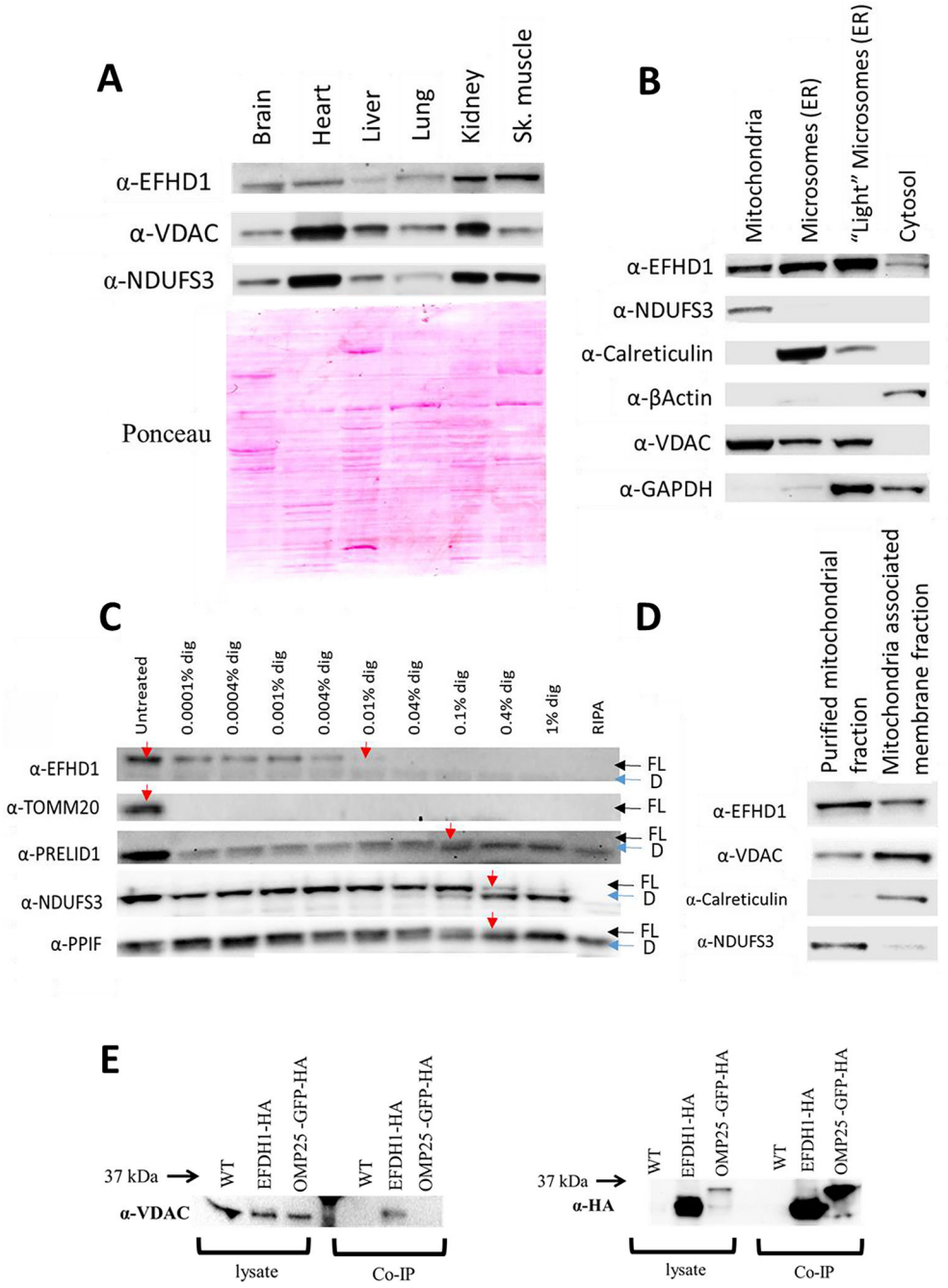

Figure 1. Tissue and subcellular distribution of EFHD1.

(A) Western blot analysis of EFHD1 in isolated mitochondria from various organs. Ponceau stain shown as loading control for total protein. VDAC and NDUFS3 show are mitochondrial outer and inner membrane proteins. (B) Western blot analysis of cellular fractions separated via differential centrifugation. Fractions were tested against known cellular biomarkers: NDUFS3 (mitochondrial inner membrane); Calreticulin (ER); β-Actin (cytosol); VDAC (outer mitochondrial membrane); and GAPDH (cytoplasm). (C) Western blot analysis of Proteinase-K assay showing the breakdown

of EFHD1 in isolated mitochondria following treatment with increasing concentrations of digitonin. Fractions were tested against known cellular biomarkers: TOMM20 (outer mitochondrial membrane); PRELID1 (mitochondrial inter-membrane space); NDUFS3 (inner mitochondrial membrane); and PPIF (mitochondrial matrix). For PRELID1, NDUFS3, and PPIF, proteinase K accessibility is revealed by shift from full-length ("FL") protein to a lower molecular weight digestion product ("D"). Red arrows show where proteins were digested. Blots are representative of >3 repeats. (D) Western blot analysis of purified mitochondrial fractions and mitochondria-associated membrane fractions. Fractions were tested against known cellular biomarkers. (E) Western blot analysis following co-immunoprecipitation of WT HAP1 cells and HAP1 cells transfected with EFHD1-HA and OMP25-GFP-HA (control). Cell lysates are shown on the left and the final elution following treatment with anti-HA beads is shown on the right. The outer membrane protein, VDAC, binds to the HA-tagged EFHD1 elution, but not to the control or WT elutions. HA tags are detected in the EFHD1-HA and control samples, but not in WT samples. Representative of 3 experiments.

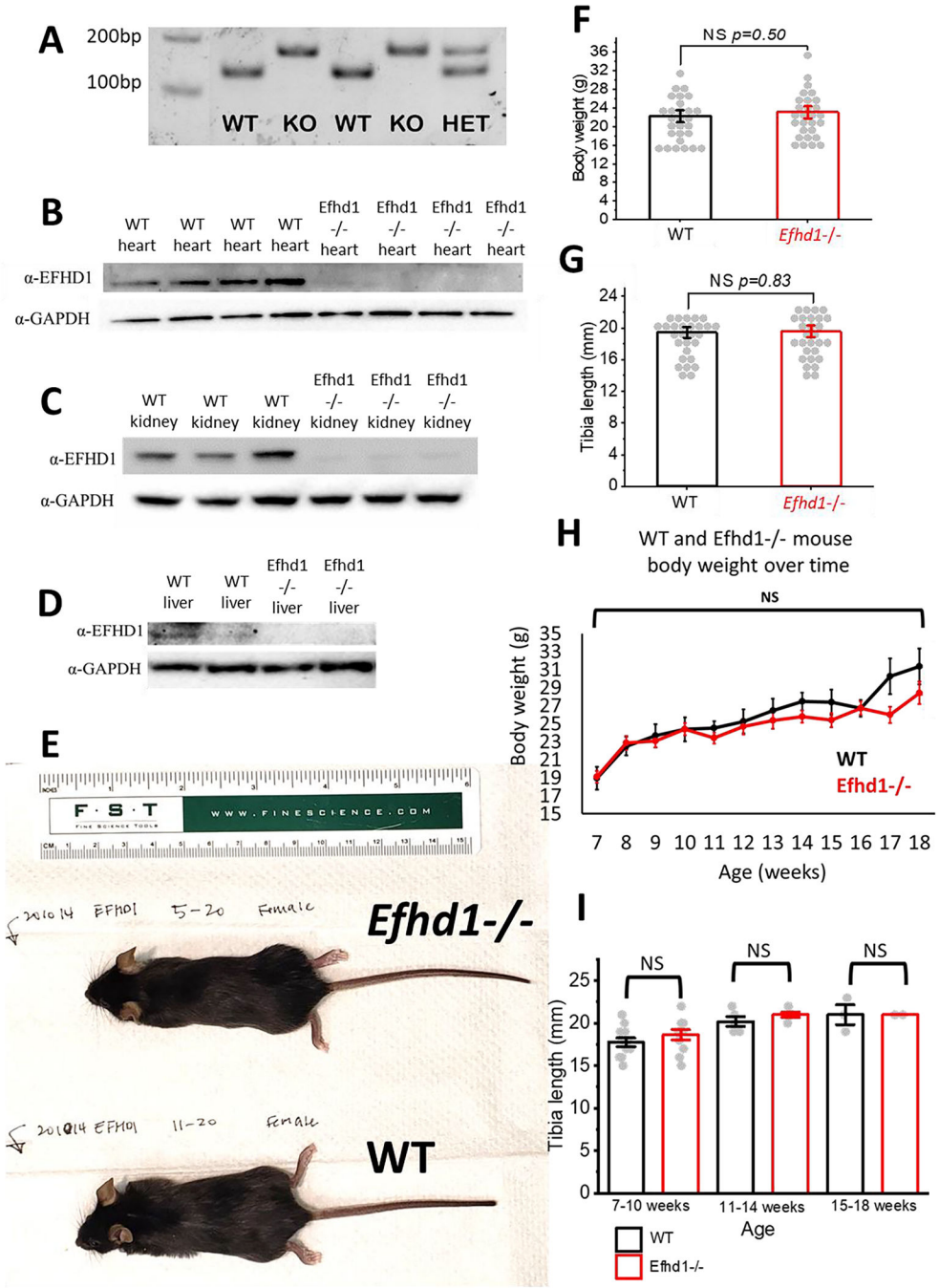

Figure 2. Basic physiology of *Efhd1*$^{-/-}$ mice is unaltered.

(A) Genotyping data confirming WT, *Efhd1*$^{-/-}$, and heterozygous mice. (B-D) Western blot analysis confirming that EFHD1 is absent in heart (B), kidney (C) and liver (D) tissue in *Efhd1*$^{-/-}$ mice. (E) Representative photo showing size similarity between WT (bottom) and *Efhd1*$^{-/-}$ (top) mice. (F-I) No difference was observed in body weight (E, n=28) or in tibia length (F, n=28). (H, I) No difference was observed in body weight or tibia length in age matched mice. All mice were young adults (7–18). Statistics: (F-H) Student's *t*-Test and (I) Mann Whitney statistical test.

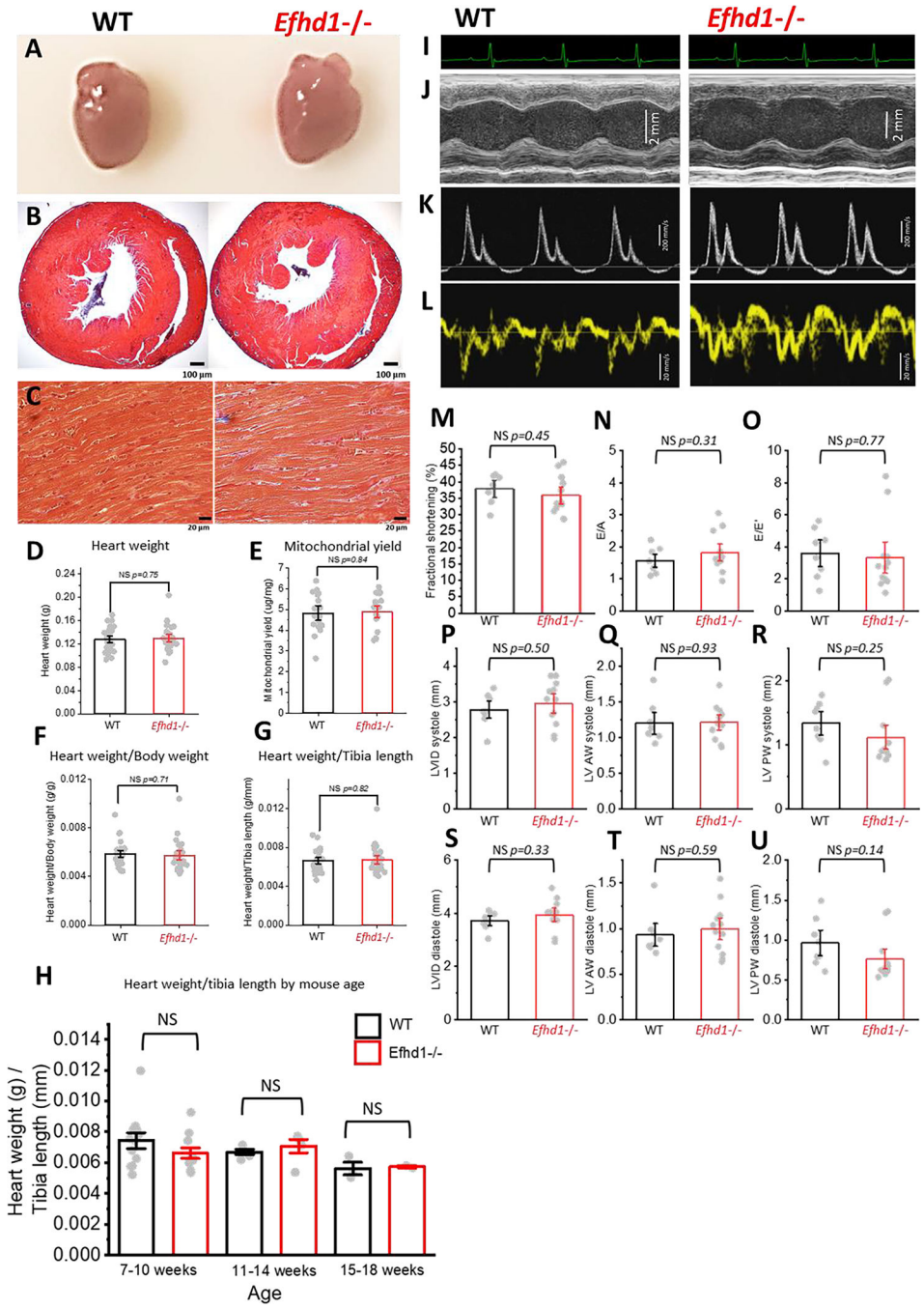

Figure 3. Basic cardiac physiology is unchanged in *Efhd1*$^{-/-}$ mice.

(A) A representative picture of WT (left) and *Efhd1*$^{-/-}$ (right) hearts taken side-by-side showing no difference in size. (B) Histology of transverse slices through WT (left) and *Efhd1*$^{-/-}$ (right) hearts. (C) High resolution histology images of WT (left) and *Efhd1*$^{-/-}$ (right) hearts treated with Masson's trichrome staining showing no difference in fibrosis levels (blue staining) in cardiomyocytes of *Efhd1*$^{-/-}$ mice compared with WT. Images are representative of 5 WT and 5 *Efhd1*$^{-/-}$ mice. (D) Comparison between heart weights of WT (black) and *Efhd1*$^{-/-}$ (red) mice (WT: n=28; *Efhd1*$^{-/-}$: n=28). (E) Comparison

of mitochondrial yield from WT (black) and *Efhd1*$^{-/-}$ (red) mouse hearts (WT: n=17; *Efhd1*$^{-/-}$: n=18). (F) Comparison of Heart weight/Body weight ratio of WT (black) and *Efhd1*$^{-/-}$ (red) mice (WT: n=28; *Efhd1*$^{-/-}$: n=28). (G) Comparison of Heart Weight/Tibia length ratio of WT (black) and *Efhd1*$^{-/-}$ (red) mice (WT: n=28; *Efhd1*$^{-/-}$: n=28). (H) No difference was observed in the heart weight/tibia length ratio in age matched mice. (I) Representative ECG recordings collected from age-matched WT (left) and *Efhd1*$^{-/-}$ (right) mice. (J) Representative m-mode echocardiogram recordings collected from age-matched WT (left) and *Efhd1*$^{-/-}$ (right) mice. (K) Representative pulse wave Doppler echocardiogram recordings showing peak velocity blood flow from left ventricular relaxation in early diastole (first peak) and peak velocity flow in late diastole caused by atrial contraction (second peak) collected from age-matched WT (left) and *Efhd1*$^{-/-}$ (right) mice. (L) Representative pulse wave Tissue Doppler echocardiogram recordings collected from age-matched WT (left) and *Efhd1*$^{-/-}$ (right) mice. H-K were taken from the same WT and *Efhd1*$^{-/-}$ mice. (M-U) Comparison of: fractional shortening (M); E/A ratio (N); E/E' ratio (O); LVID during systole (P); LVAW during systole (Q); LVPW during systole (R); LVID during diastole (S); LVAW during diastole (T); LVPW during diastole (U); in WT (red) and *Efhd1*$^{-/-}$ (black) mice measured from echocardiograms. WT: n=8; *Efhd1*$^{-/-}$: n=12. Histological and echocardiogram data were collected from age-matched 18-week old mice. Statistics: (D-G) Student's T-Test and (H,M-U) Mann-Whitney statistical test.

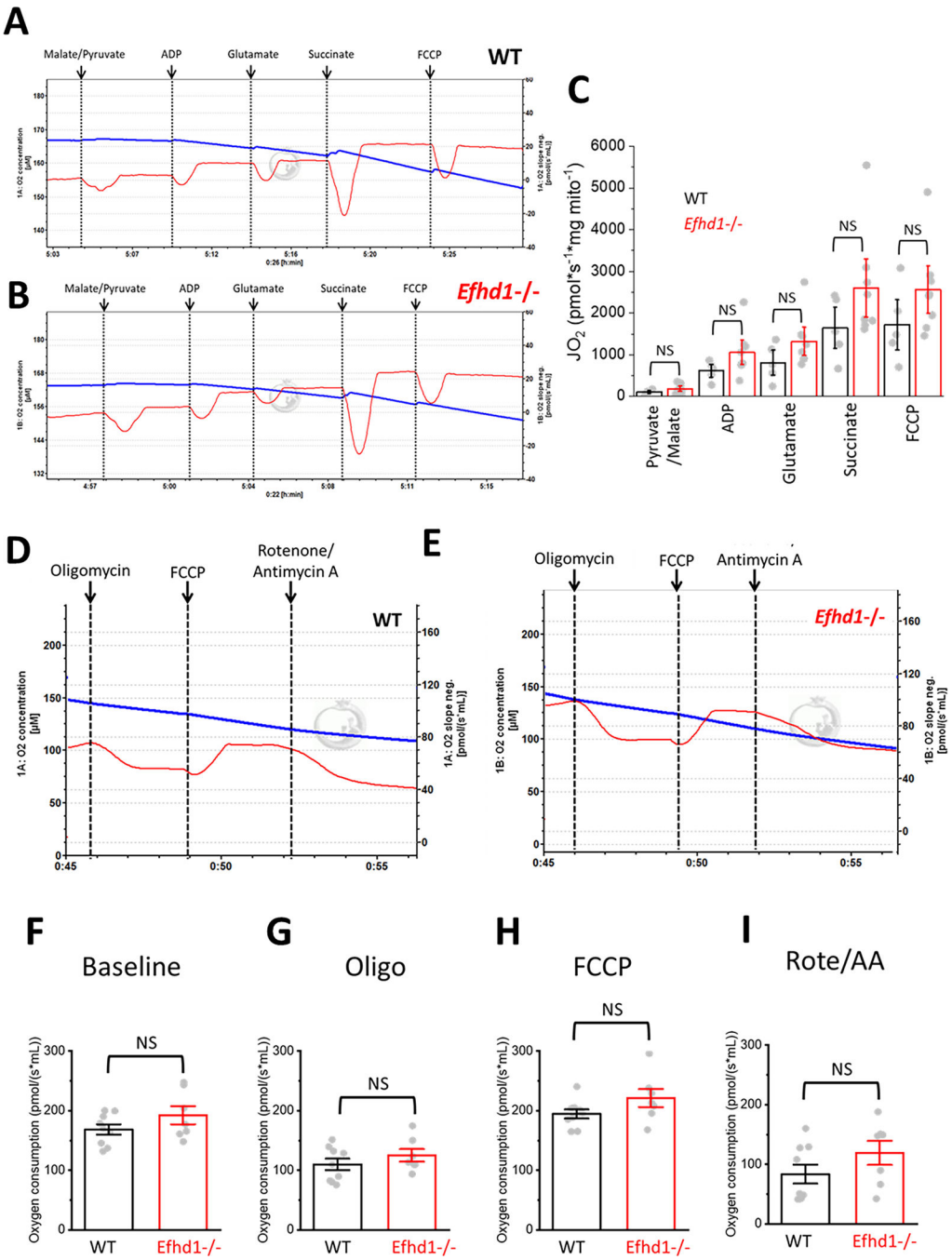

Figure 4. Respiration in mitochondria and whole cardiomyocytes from *Efhd1*$^{-/-}$ mice.

(A, B) Representative traces from an Oroboros O2k-FluoRespirometer showing oxygen consumption in mitochondria isolated from WT (A) and *Efhd1*$^{-/-}$ (B) hearts in response to respiratory substrates. The blue line represents oxygen levels. The red line represents rate of oxygen consumption. (C) Comparison of the rate of oxygen consumption of mitochondria from WT (black) and *Efhd1*$^{-/-}$ (red) in the presence of respiratory substrates. (H) Comparison of the respiratory acceptor control ratio (RCR) in mitochondria from WT (black) and *Efhd1*$^{-/-}$ (red). WT: N=5; *Efhd1*$^{-/-}$: N=8. (D, E) Representative traces from

an Oroboros O2k-FluoRespirometer showing oxygen consumption in whole cardiomyocytes isolated from WT (D) and *Efhd1*$^{-/-}$ (E) hearts in response to respiratory inhibitors. The blue line represents oxygen levels. The red line represents rate of oxygen consumption. (F-I) Comparison of the rate of oxygen consumption of whole cardiomyocytes from WT (black) and *Efhd1*$^{-/-}$ (red) in the presence of respiratory inhibitors. Oligo = Oligomycin; FCCP = Carbonyl cyanide-p-trifluoromethoxyphenylhydrazone; Rote/AA = Rotenone/Antimycin A. WT, n=9; KO, n=7. Statistics: Mann-Whitney statistical test.

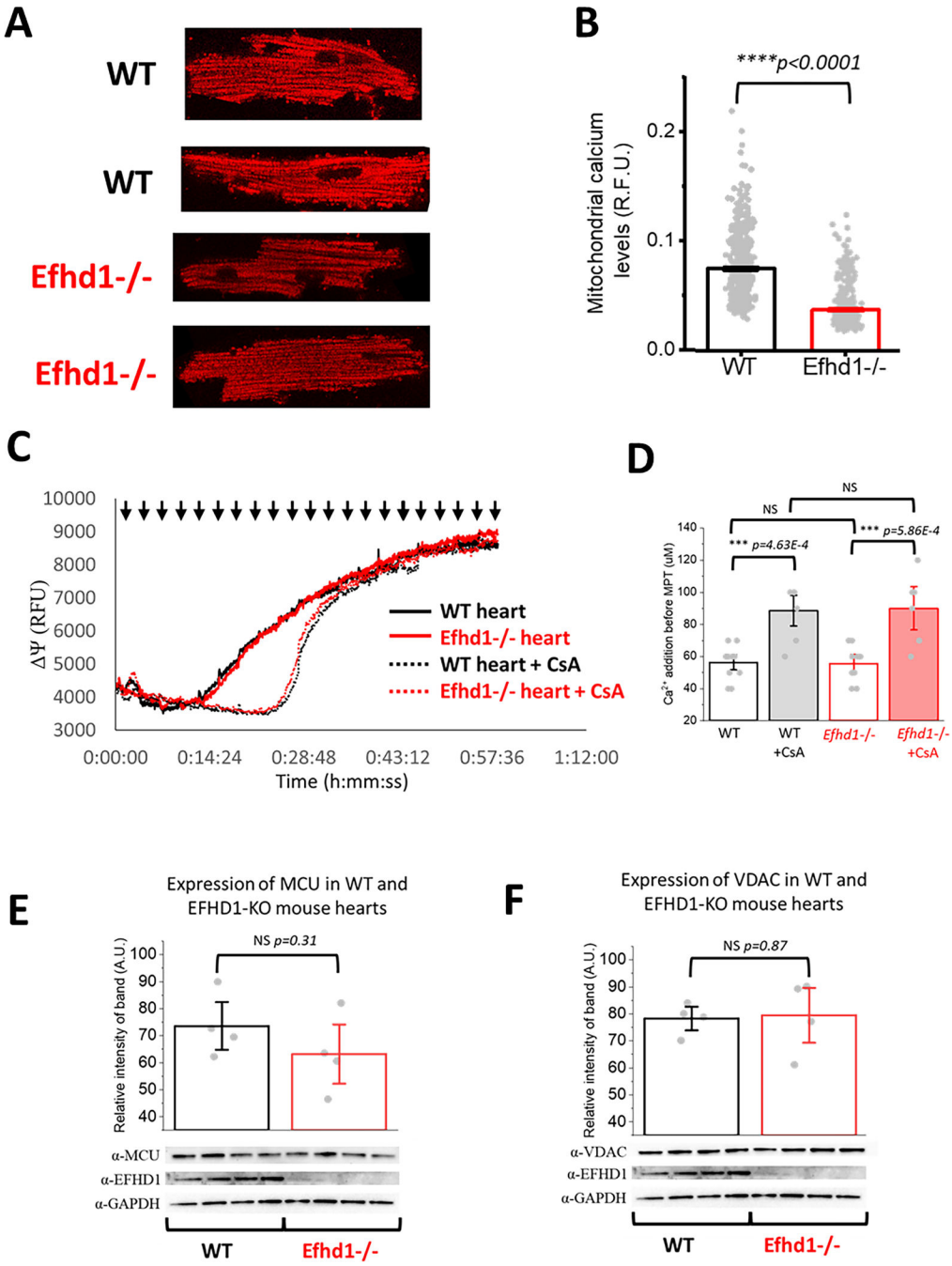

Figure 5. Efhd1−/− cardiomyocytes exhibit lower mitochondrial calcium levels, but calcium retention capacity and calcium uptake machinery levels unchanged.

(A) Representative images showing isolated WT and Efhd1−/− cardiomyocytes stained with the mitochondrial Ca^{2+} sensor, XRhod1. (B) Changes in mitochondrial Ca^{2+} levels following XRhod1 staining in isolated WT and *Efhd1*$^{-/-}$ cardiomyocytes in the presence of 1 mM extracellular Ca^{2+} (C) A representative calcium retention trace of mitochondria isolated from WT (black) and *Efhd1*$^{-/-}$ (red) mouse hearts in the presence and absence of 10 μM Cyclosporin A (CsA). Black arrows indicate 5 μM Ca^{2+} injections. Mitochondrial viability was measured as ΔΨ/TMRM fluorescence. (D) Comparison of calcium retention

before the triggering of an MPT event in WT and *Efhd1*$^{-/-}$ mice in the presence and absence of CsA. WT: n=11; WT+CsA: n=7; *Efhd1*$^{-/-}$: n=9; *Efhd1*$^{-/-}$ +CsA: n=6. Mitochondrial viability was measured as ΔΨ/TMRM fluorescence. (E) Relative expression of the mitochondrial calcium uniporter (MCU) in WT and *Efhd1*$^{-/-}$ mouse hearts. (F) Relative expression of the voltage-dependent anion channel (VDAC) in WT and *Efhd1*$^{-/-}$ mouse hearts. Statistics: (B) Students T-Test, (D) 1-way ANOVA with a Bonferroni post-test, (E,F) Mann-Whitney statistical test.

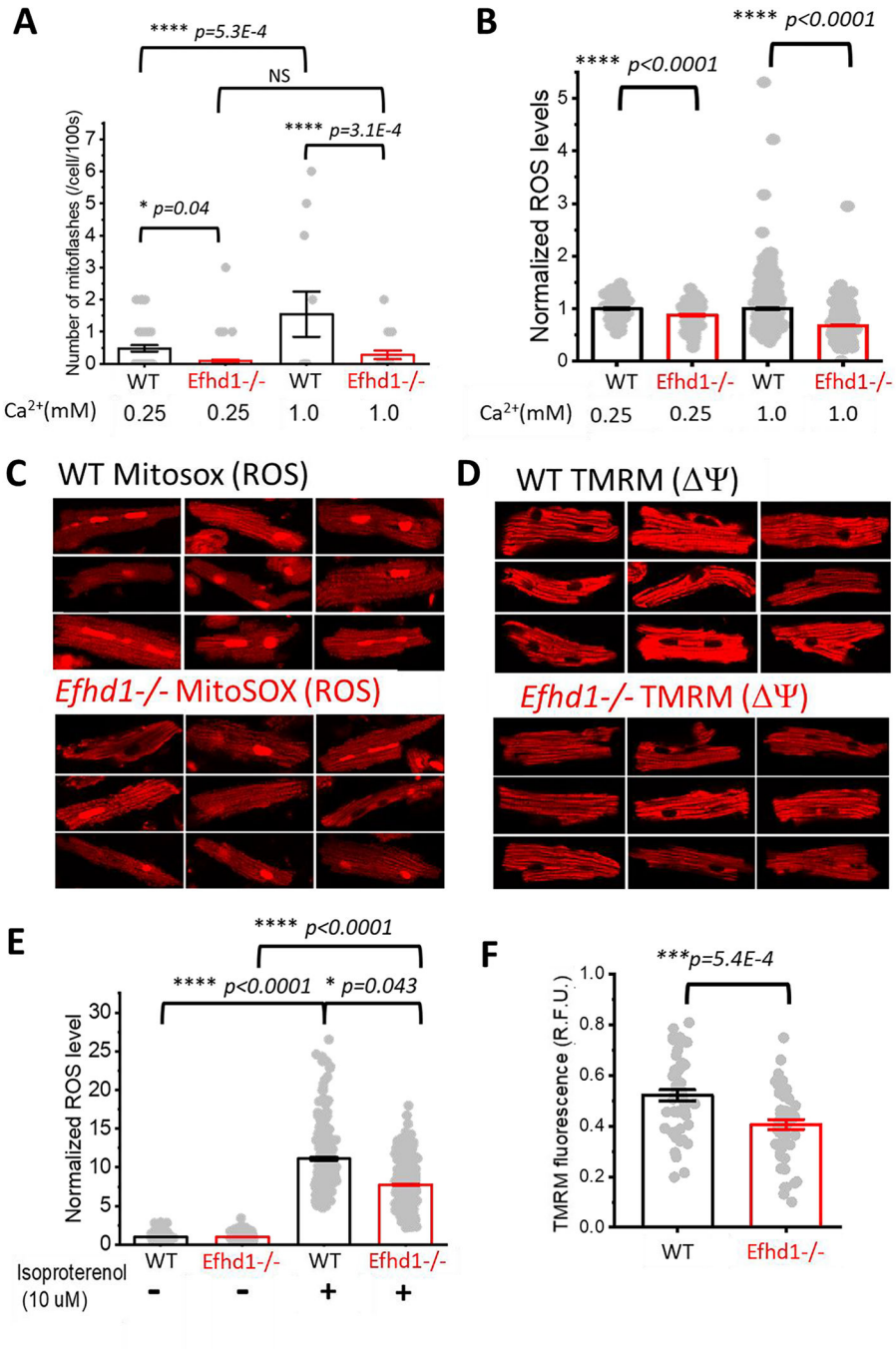

Figure 6. Mitoflash frequency, ROS levels, and ΔΨ are decreased in *Efhd1*$^{-/-}$ mouse cardiomyocytes.

(A) Comparison of mitoflash frequency between isolated cardiomyocytes from WT and *Efhd1*$^{-/-}$ mice in the presence of either 0.25 mM extracellular Ca^{2+} (WT, n=50; *Efhd1*$^{-/-}$, n=79) or 1 mM extracellular Ca^{2+} (WT, n=11; *Efhd1*$^{-/-}$, n=18). (B) Comparison of ROS levels measured as relative MitoSOX fluorescence in isolated WT and *Efhd1*$^{-/-}$ cardiomyocytes in the extracellular presence of 0.25 mM Ca^{2+} (WT, n=132; *Efhd1*$^{-/-}$, n=125), or 1mM Ca^{2+} (WT, n=1501; *Efhd1*$^{-/-}$, n=757). (C) Representative images of cardiomyocytes from WT (top) and *Efhd1*$^{-/-}$ (bottom) mice stained with MitoSOX, a

ROS reporter. (D) Representative images of cardiomyocytes from WT (top) and *Efhd1*$^{-/-}$ (bottom) mice stained with Tetramethylrhodamine, methyl ester (TMRM), a ΔΨ reporter. (E) Comparison of ROS levels measured as MitoSOX fluorescence normalized to control (vehicle, DMSO) in isolated WT and *Efhd1*$^{-/-}$ cardiomyocytes in the extracellular presence of DMSO (WT, n=309; *Efhd1*$^{-/-}$, n=503) and 10 uM isoproterenol (WT, n=269; *Efhd1*$^{-/-}$, n=941). (F) Comparison of ΔΨ measured as relative TMRM fluorescence in WT and *Efhd1*$^{-/-}$ in the extracellular presence of 0.25 uM Ca^{2+} (WT, n=51; *Efhd1*$^{-/-}$, n=52). Statistics: All experimental n values represent the number of cardiomyocytes isolated from a minimum of 2 mice for each. (A,B,F) Students T-Test, (E) 1-way ANOVA with a Bonferroni posttest.

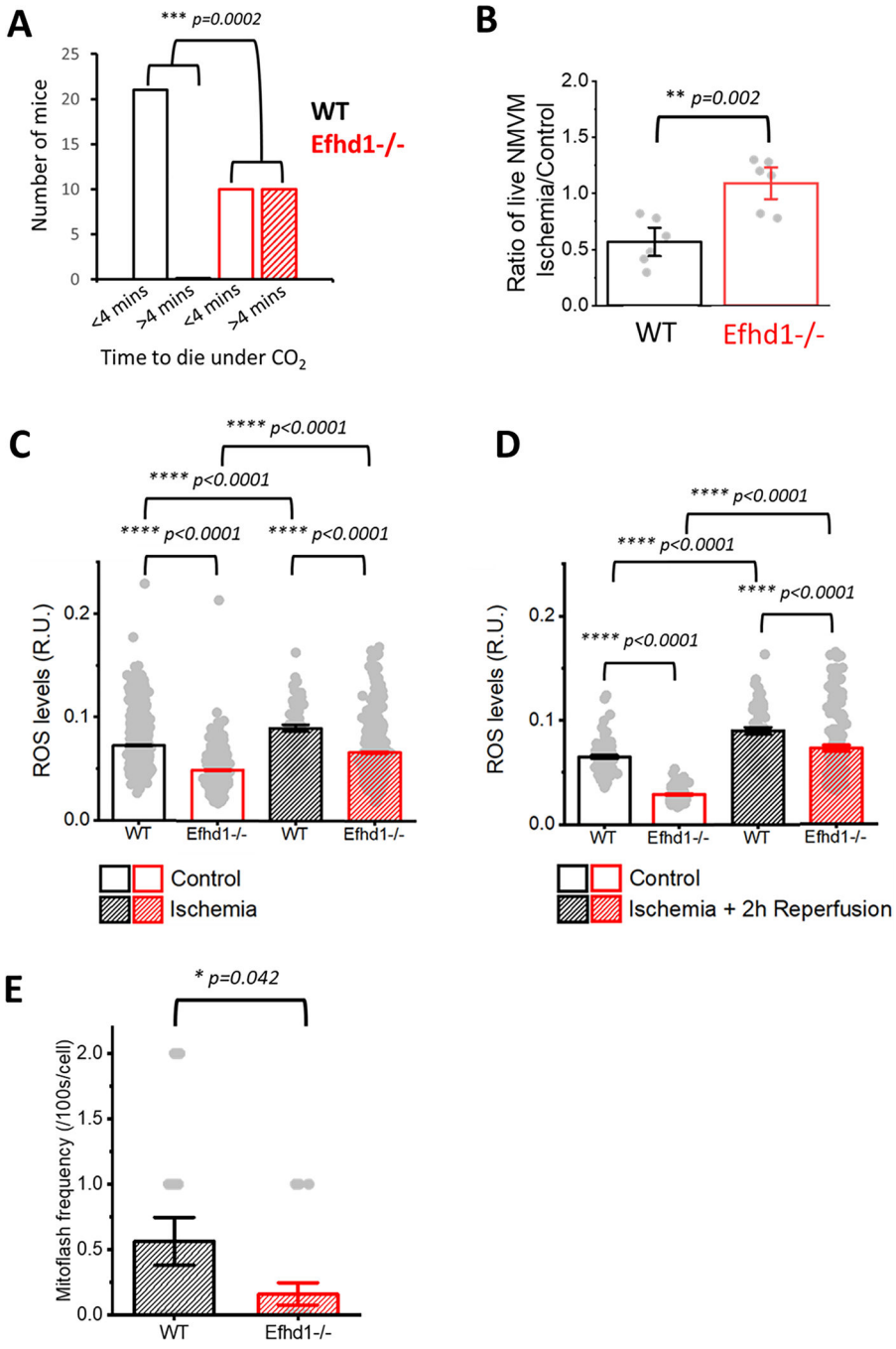

Figure 7. *Efhd1*$^{-/-}$ mice are resistant to hypoxia and ischemia/reperfusion.

(A) Comparing the number of WT (black) and *Efhd1*$^{-/-}$ (red) mice which died in less than 4 mins exposure to CO_2 with the number which took longer than 4 mins to die (WT n=21; *Efhd1*$^{-/-}$ n=20). (B) Comparison of resistance to simulated ischemia-reperfusion in cultured neonatal mouse ventricular myocytes (NMVMs) isolated from 1-day old WT (black) and *Efhd1*$^{-/-}$ (red) mouse pups. WT: N=6; *Efhd1*$^{-/-}$: N=6, where each "N" represents NMVMs isolated from one litter (3–10 pups). (C) Comparison of ROS levels in isolated adult WT and *Efhd1*$^{-/-}$ cardiomyocytes immediately following simulated ischemia (WT, control, n=1501,

I/R, n=61; *Efhd1*$^{-/-}$, control, n=757; I/R, n=671). (D) Comparison of resistance to ROS levels in isolated adult WT and *Efhd1*$^{-/-}$ cardiomyocytes following simulated ischemia with 2 hours' reperfusion (WT, control, n=104, I/R, n=61; *Efhd1*$^{-/-}$, control, n=99; I/R, n=157). (E) Comparison of mitoflash frequency in WT and *Efhd1*$^{-/-}$ cardiomyocytes following 30 mins ischemia and 30 mins reperfusion (WT, n=16; *Efhd1*$^{-/-}$, n=19). Statistics: (A) Fisher Exact; (B) Mann-Whitney statistical test; (C, D) 1-way ANOVA with a Bonferroni posttest; (F) Student's T-Test.